ACTA IMEKO
ISSN: 2221-870X
September 2026, Volume 15, Number 3, 1 - 18

Dynamic Finite Element Modelling (DFEM) procedure for cultural heritage: Displacement-based reconstruction of the dynamical behaviour of the Roman bridge over the Savuto River

Fabrizio Barone[1], Armando Di Maio[2], Salvatore Antonio Fornaro[3], Marco Casazza[1]

[1] *University of Salerno, Department of Medicine, Surgery and Dentistry "Scuola Medica Salernitana", Via Salvador Allende 43, 84081 Baronissi, Italy*
[2] *Studio di Architettura Di Maio, Napoli, Italy*
[3] *Studio di Architettura Fornaro, Sapri, Italy*

ABSTRACT
This study presents a metrological approach for investigating cultural heritage structures through Dynamic Finite Element Modelling (DFEM) procedure and displacement-based vibroacoustic monitoring. The Roman bridge over the Savuto River, Calabria, Italy, built in the 2nd century BC along the Via Popilia, is analysed as a case study. Broadband mechanical seismometers were deployed to measure linear and angular displacements under ambient excitation, allowing modal frequencies, thermal deformation cycles, and local dynamic anomalies to be identified. The comparison between measured responses and numerical predictions showed good agreement for the main vibration modes, while persistent low-frequency discrepancies indicated that the visible geometry alone does not fully describe the structural system. These results support the hypothesis of an additional concealed substructure beneath the riverbed, and reveal asymmetric behaviour associated with twentieth-century restoration interventions. The study shows how high-sensitivity measurements can strengthen digital modelling by transforming dynamic response into metrological evidence for structural diagnosis and heritage interpretation.

Section: RESEARCH PAPER

Keywords: Dynamic Finite Element Modelling; cultural heritage; vibroacoustic monitoring; displacement-based sensing; Roman bridge; digital twin; Roman archaeology

Citation: F. Barone, A. Di Maio, S. A. Fornaro, M. Casazza, Dynamic Finite Element Modelling (DFEM) procedure for cultural heritage: Displacement-based reconstruction of the dynamical behaviour of the Roman bridge over the Savuto River, Acta IMEKO, vol. 15 (2026) no. 3, pp. 1-18. DOI: 10.21014/actaimeko.v15i3.2386

Section Editor: Fabio Leccese, Università Degli Studi Roma Tre, Rome, Italy

Received April 28, 2026; **In final form** September 1, 2026; **Published** September 2026

Funding: This work did not receive any financial support.

Corresponding author: Fabrizio Barone, e-mail: fbarone@unisa.it

1. INTRODUCTION

Cultural heritage structures pose a specific metrological problem. Their visible geometry, material composition, internal configuration, and boundary conditions are often only partially known, while their present behaviour reflects centuries of environmental interaction, degradation, repair, and transformation. For this reason, conventional approaches based only on survey documentation or finite element modelling may provide an incomplete representation of the real structural system.

In this context, physical metrology can support the quantitative assessment of research hypotheses in historical, archaeological, and cultural heritage studies [1]–[3]. Within a multidisciplinary framework, documentary sources, archaeological interpretation, and material evidence provide the initial basis for formulating historically plausible hypotheses concerning the functions of artefacts and built structures, the needs to which they responded, and the practical knowledge involved in their conception and construction. Measurements of relevant physical quantities can then be used to assess the compatibility of such hypotheses with the observed behaviour of the material object, the structure, or the space under investigation. In particular, previous studies show that physical metrology can provide quantitative evidence also for investigating the functional purposes, empirical practices, and non-codified technical knowledge embodied in material forms. Such experience-based practical knowledge may be understood through the concept of téchne, in the sense attributed to the term in ancient Greek culture.

The present study addresses this problem through the Dynamic Finite Element Modelling (DFEM) procedure [4]–[6]. DFEM is proposed as a metrological procedure in which the numerical model and the measurement configuration are developed through mutual optimisation. The preliminary FEM is used as a first physically plausible estimate to support the design of the monitoring system, while the measured response is used to update both the model parameters and, when necessary, the spatial configuration of the sensors.

This approach is applied to the Roman bridge over the Savuto River, a structure whose apparent formal simplicity conceals a complex interaction among geometry, materials, hydraulic conditions, foundation behaviour, and long-term transformations. The case study is particularly relevant because the monument cannot be investigated through invasive procedures, and the measurement configuration must therefore be compatible with conservation, access, and operational constraints. The aim of the paper is to show how displacement-based vibroacoustic monitoring, combined with adaptive finite element modelling, can reconstruct the dynamic behaviour of the bridge, and transform residual discrepancies between model and measurement into metrological evidence for structural and historical interpretation.

2. METHODOLOGY

2.1. Conceptual background of the metrological method

The Dynamic Finite Element Modelling (DFEM) procedure, schematised in Figure 1, is based on the mutual optimisation of two coupled components: the numerical model and the measurement configuration. A preliminary FEM, developed from archaeological, geometric, historical, and technical information, provides the first estimate of the expected dynamic behaviour, and supports the initial definition of sensor typology,

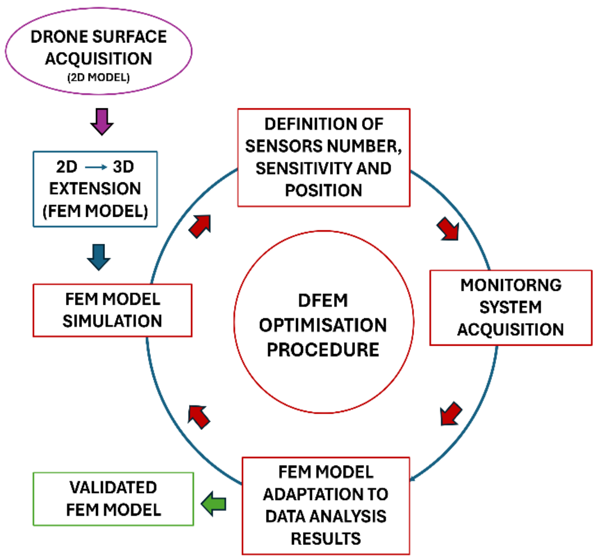

Figure 1. DFEM procedure model–measurement loop.

sensitivity, bandwidth, number, orientation, and position. The acquired response is then used to update the uncertain model parameters, including mass distribution, stiffness, and boundary conditions, and to verify whether the adopted sensor layout provides sufficient spatial observability of the relevant dynamic features.

Although DFEM is based on well-established methods documented in the literature, it should not be understood as a conventional model-updating procedure, nor as a Structural Health Monitoring procedure alone. Its objective is to organise measurement and modelling within the same metrological process, so that the dynamic response is used not only as a diagnostic indicator, but also as physical evidence for reconstructing how the monument behaves as a structural system.

This point is particularly relevant for cultural heritage structures, where the geometry, material properties, boundary conditions, and internal configuration are often only partially known. In such cases, measurement cannot be treated as merely ancillary to the numerical model. Unlike new structures, for which geometry, materials and technical characteristics are generally defined by design, historical monuments require a reciprocal process in which the preliminary model supports the first configuration of the measurement system, and the measured response progressively constrains the interpretation of the model.

Therefore, persistent discrepancies between model predictions and measured response are not interpreted only as modelling errors. When stable, spatially coherent, and mechanically admissible, they become metrological evidence of possible insufficient observability, hidden structural components, altered constraints, local discontinuities, restoration effects, or undocumented construction solutions. Modal frequencies, rotational anomalies, thermal deformation cycles, and inconsistencies between visible geometry and dynamic behaviour can consequently support both structural interpretation and archaeological hypotheses.

In this sense, DFEM extends vibration metrology beyond its conventional diagnostic application. It provides a procedure for linking the material behaviour of the structure to the intangible technical knowledge embedded in it. For a historical bridge, this includes the constructive logic of its builders, the empirical adaptation to river flow, temperature cycles, soil–foundation interaction, and long-term changes in boundary conditions. This practical construction knowledge corresponds to ancient téchne, understood here not as an abstract symbolic layer, but as non-codified technical competence materialised in the built form.

The same principle also clarifies the role of digital models in heritage science. BIM environments, digital twins, and AI-based reconstructions are useful only if constrained by high-quality measurements. Within DFEM, the digital model is not an autonomous representation, but a physically informed and continuously verifiable interface between the monument and its scientific interpretation. Previous applications to monuments, such as the Trajan arch in Benevento or the temple of Neptune in Paestum, have shown that high-sensitivity monitoring can reveal structural and functional properties not accessible through visual inspection alone [7]–[9]. In these cases, the integration of distributed sensing and adaptive modelling makes it possible to reconstruct dynamic behaviours related to historical use, environmental exposure, and construction logic.

The DFEM workflow can be summarised in five phases. First, technical data from surveys, previous documentation, and reliable sources are collected to support the initial system design [5]. Second, a preliminary digital model is developed from the available geometric and historical information and used as a first estimate for defining sensor specifications and initial measurement locations [10]–[12]. Third, the preliminary monitoring configuration is installed and operated under the operational constraints imposed by the heritage asset. Fourth, natural frequencies, frequency response functions, and relevant phase or rotational features are extracted from the measured data and used to refine both the FEM parametrisation and the sensor configuration [13], [14]. Finally, the optimisation process ends when the model predictions and the measurement configuration satisfy the required accuracy, precision, and observability criteria. At this stage, the monitoring system reaches the best feasible configuration within the conservation and access constraints of the site, including the need to cover the broadband and sub-hertz response induced by natural and anthropic excitation sources.

2.2. DFEM metrological procedure

The DFEM procedure was applied to the Savuto River bridge to overcome a limitation of geometry-based modelling: the visible configuration alone may not reproduce the actual dynamic behaviour of a historical structure. The procedure therefore evaluates the FEM and the measurement system together. The preliminary model defines the first dynamic hypothesis and guides the initial sensor layout; the measured response then tests both the model assumptions and the spatial observability provided by the adopted measurement configuration.

In the present case, the optimisation process showed that the visible-geometry FEM and the available sensor configuration did not fully reproduce all measured resonance features, especially in the low-frequency range. This mismatch was treated as residual metrological information. It may indicate incomplete sensor observability, uncertain mass or stiffness distribution, altered constraints, restoration effects, local discontinuities, or non-visible structural components beneath the riverbed. One mechanically admissible hypothesis is the presence of additional mass and/or stiffness associated with the foundation system. This interpretation is compatible with previous archaeological suggestions, but remains a dynamically grounded hypothesis requiring further verification, not direct archaeological proof.

In the present application, the DFEM workflow was organised according to the following operational steps: 1. Construction of a preliminary finite element model from the visible geometry obtained by survey and from available historical and archaeological information; 2. Definition of the main uncertain assumptions, including effective mass distribution, stiffness distribution, support conditions, and possible foundation-related constraints; 3. Acquisition of displacement-based signals under ambient excitation through a non-invasive sensor layout; 4. Identification of stable frequency peaks and phase or rotational features from the measured time histories; 5. Comparison between measured dynamic features and numerical modal predictions; 6. Assessment of whether the number and spatial distribution of measured channels are sufficient to observe the identified modal features; 7. Constrained revision of the model assumptions and, when necessary, reconsideration of the measurement configuration; 8. Interpretation of persistent residual discrepancies as possible indicators of incomplete sensor observability, non-visible masses, altered constraints, local discontinuities, restoration effects, or undocumented constructive solutions. The procedure begins with the construction of an initial FEM based on all available archaeological, historical, geometric, and material data. In the case of the Savuto bridge, this preliminary model was derived from aerial survey data, direct observation, and existing historical documentation. At this stage, the model provides a plausible but incomplete approximation of the structure, including its apparent mass distribution, geometry, and boundary conditions.

Then, this initial model is compared with the results of the monitoring campaign. The distributed sensing system records linear and angular displacements over time, capturing natural vibration modes, resonance frequencies, and cyclic deformations associated with environmental forcing, particularly thermal variations between day and night. Spectral analysis of the acquired signals enables the identification of stable modal peaks representing the true structural dynamics of the monument.

At this stage, the relationship between the measured frequency peaks and the sensor layout becomes a central metrological issue. Stable peaks in the spectral density indicate the presence of dynamically relevant modal features in the investigated frequency range. However, a frequency peak is not equivalent to a complete modal identification. A single sensor may detect several peaks, but it cannot reconstruct the spatial structure of the corresponding mode shapes, nor can it reliably distinguish closely spaced modes, phase relationships or local rotational components.

If the measured response is expressed in modal form, the vector of measured outputs can be written as:

$$\mathrm{y}(t) = \Phi_s \, \mathrm{q}(t) + \mathrm{e}(t), \tag{1}$$

where $\mathrm{y}(t)$ is the vector of measured signals, Φ_s is the modal matrix observed at the sensor locations, $\mathrm{q}(t)$ is the vector of modal coordinates, i.e. the time-dependent amplitudes of the identified vibration modes, and $\mathrm{e}(t)$ represents measurement noise and unmodelled components. If m target modes have to be distinguished in the frequency band of interest, the observed modal matrix must have sufficient rank:

$$rank(\Phi_s) = m \, . \tag{2}$$

Since $\Phi_s \in \mathbb{R}^{q \times m}$, where q is the number of independent measured degrees of freedom, this condition implies the necessary lower-bound requirement:

$$q \geq m \, . \tag{3}$$

Therefore, the number of independent measured channels should not be lower than the number of target modes to be distinguished. This is only a minimum observability condition. In practice, a larger number of measured points is generally required to reconstruct mode shapes, phase relationships, rotational components, closely spaced modes, and local dynamic anomalies.

This requirement links DFEM to the literature on Optimal Sensor Placement, although the aim of DFEM is not limited to damage detection. In modal identification, sensor placement is commonly formulated as the problem of selecting measurement locations that maximise the information content and the linear independence of the observed modal partitions. Effective Independence methods select sensor positions according to their contribution to the linear independence of target modes [15], while information-based approaches evaluate how different sensor configurations reduce uncertainty in the identification of structural parameters [16]. These principles are directly relevant to DFEM, because the sensor layout determines which part of the monument's dynamic behaviour can be observed and, consequently, which model parameters or hidden features can be meaningfully inferred. The same issue is particularly evident in Operational Modal Analysis approaches based on Blind Source Separation [17]. In these methods, the measured responses are treated as mixtures of modal sources that have to be separated from output-only data. Conventional BSS-based OMA formulations generally require a determined or overdetermined problem, meaning that the number of sensors must be at least equal to the number of active modes in the frequency range of interest in order to avoid spatial aliasing. When this condition is not satisfied, the identification problem becomes underdetermined and additional assumptions, sub-band decomposition strategies or repeated measurement configurations are required.

The core of the DFEM procedure lies in the mutual optimisation of two coupled components: the digital dynamic model and the physical measurement configuration. The process is not limited to the iterative minimisation of discrepancies between measured and predicted responses by modifying FEM parameters. Such a one-way strategy would reduce the procedure to conventional model updating and would implicitly assume that the measurement system is already adequate. In DFEM, discrepancies between numerical predictions and experimental evidence are instead used in two complementary ways. First, they guide the refinement of mechanically admissible model parameters, such as stiffness distribution, mass distribution, and boundary conditions. Second, they guide the refinement of the measurement configuration itself, including the number, position, directionality, sensitivity, and bandwidth of sensors. The process is therefore not a simple calibration of a pre-existing model, but a recursive metrological interaction between simulation and observation.

The adequacy of the measurement system is therefore determined not only by the number and position of sensors, but also by their metrological quality. In low-amplitude ambient-vibration testing of massive historical structures, modal peaks may be weak, closely spaced or partially masked by environmental noise. Sensor sensitivity, bandwidth, self-noise, transfer-function stability, and low-frequency performance directly affect the ability to identify true modal features and to reject spurious peaks. In DFEM, poor metrological quality cannot be compensated simply by modifying FEM parameters, because the model would then be adjusted to incomplete or unreliable experimental evidence.

This iterative adaptation leads to the emergence of a dynamically consistent digital twin. Such a model is not merely a virtual representation, but a metrologically validated construct capable of reproducing observed behaviour and revealing structural features not directly accessible through visual inspection.

Furthermore, the procedure allows the identification of local dynamic anomalies that may be associated with later interventions, environmental forcing, or altered boundary conditions. By analysing phase relationships and rotational behaviour across different parts of the structure, DFEM can distinguish between coherent global motion and localised asymmetries resulting from altered boundary conditions. This is particularly relevant in structures that have undergone restoration, where modern interventions may significantly influence dynamic behaviour without being immediately visible.

Accordingly, the output of DFEM is not a numerical model alone, but an optimised model–measurement configuration. This configuration defines which dynamic features can be reliably observed, which model parameters can be updated, and which residual discrepancies require further structural, archaeological, or metrological investigation.

3. MONITORING SYSTEM

3.1. Sensors and system architecture

The implementation of the DFEM procedure required the development of a distributed monitoring system specifically configured to acquire highly reliable data on the structural dynamics of the bridge. Within this framework, the monitoring system is not a secondary technical support, but an active component of the DFEM metrological procedure. The quality, sensitivity, bandwidth, and adaptability of the measurement system directly determine the possibility of developing a numerical model capable of accurately reproducing the real behaviour of the heritage structure.

For this reason, the monitoring architecture adopted for the Savuto bridge derives from a broader family of systems, previously developed and tested on a range of historical monuments, including the Arch of Trajan in Benevento, the Temple of Neptune at Paestum, where a permanent monitoring system of this type is operated by the National Archaeological Park of Paestum and Velia, historic worship spaces, chamber music environments, cave churches, and medieval bell towers [5],[7]–[9],[18].

The monitoring solution implemented for the Savuto River bridge was designed as a simplified yet highly effective distributed modular system. Owing to administrative and operational constraints related to the protection of the monument, the configuration was limited to a maximum of sixteen structural degrees of freedom, corresponding to eight dominant linear and eight angular components. Despite this limitation, the system provided data of sufficient quality to support the DFEM optimisation process and to reveal significant structural features. The modularity of the system, schematically represented in Figure 2, is based on a standard Ethernet network architecture connecting local 24-bit data acquisition (DAQ) units (see Table 1 for technical details of the DAQ unit). These units can be arranged using standard or hybrid daisy-chain and star configurations, allowing flexible deployment according to the geometry of the monitored structure. For the present application, the acquisition units were National Instruments™ FieldDAQ devices (model FD-11603), each providing up to eight simultaneously sampled 24-bit analogue input channels,

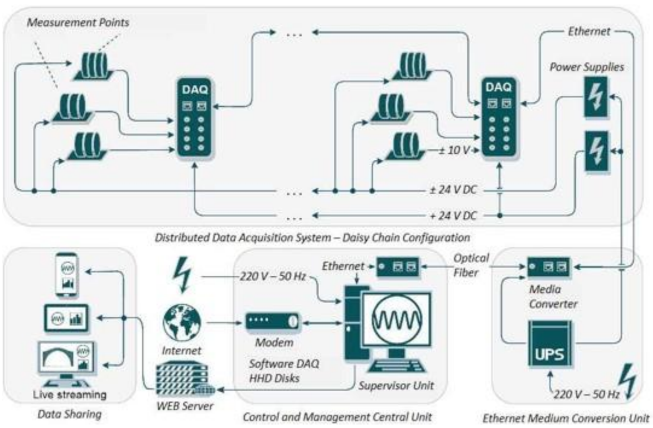

Figure 2. Schematic structure of the configuration of the distributed monitoring system used for monitoring the Roman bridge over the Savuto River.

Table 1. Main characteristics of the DAQ unit, Model FD-11603 from National InstrumentsTM.

Channel Number	**8 channels – analogic input**
ADC type	24 bits – Delta Sigma
Input Voltage Range	± 10.5 V
Maximum Sampling Rate	102.4 kSamples/s
Sampling Typology	Simultaneous
Accuracy	± 30 ppm max

with maximum sampling rates of approximately 100 kSamples/s and high metrological accuracy.

The entire monitoring system was battery-powered in order to minimise electromagnetic interference and improve the signal-to-noise ratio during field measurements. System management, synchronisation, acquisition control, and real-time visualisation were handled through a dedicated graphical interface (Supervisor) developed by Adv3S™, operating on a workstation environment. This platform enabled remote configuration of the acquisition units, real-time monitoring of sensor outputs, and full management of the measurement campaigns throughout the successive DFEM optimisation stages.

A critical aspect of monitoring architecture concerns sensor selection. For the Savuto bridge, the system employed broadband monolithic mechanical seismometers (model SE-10HL, see Figure 3), produced by Advanced Scientific Sensors and Systems (Adv3S™) [19]–[21].

These instruments, whose technical details are synthesized in Table 2, belong to a class of high-sensitivity folded-pendulum sensors based on monolithic mechanical architecture and LVDT readout, capable of detecting extremely small linear displacements and angular variations over a wide frequency range extending from DC to 100 Hz. Their spectral sensitivity, better than 10^{-8} m/√Hz within the relevant frequency interval, makes them particularly suitable for heritage monitoring applications in which structural responses are subtle, low-frequency, and strongly influenced by environmental excitation.

The higher effectiveness of the chosen sensor type depends on different metrological factors. From one side, the physical variable of interest for the purpose of this research is the structural response in terms of broadband small-amplitude vibrations, including the lower frequencies, where the quality of the measurement output is strongly governed by transfer function, low-frequency sensitivity, signal-to-noise ratio, and

Figure 3. Model SE-10HL mechanical seismometer produced by Advanced Scientific Sensors and Systems (Adv3STM).

Table 2. Main features of the SE-10HL model seismometer, produced by Adv3STM.

Architecture	Model SE-10HL – class EB-100 Monolithic Folded Pendulum (Pat.)
Configuration	Seismometer (without feedback)
Natural Frequency	3.80 Hz ± 10%
Readout	LVDT
Band	DC – 100 Hz
Sensitivity	72 V/mm ± 10%
Spectral Sensitivity	< 10^{-8} m/$\sqrt{\text{Hz}}$ (3.5 Hz < f < 100 Hz)
Output Signal (dual)	± 10 V (range)

post-processing robustness [22]–[24]. In the case of cultural heritage and archaeological structures, this issue becomes even more relevant because operational modal analysis based on ambient vibration is especially appropriate when artificial excitation should be avoided, since it enables dynamic identification under non-invasive operating conditions, and limits potentially harmful interactions with the asset [25], [26]. In accelerometric measurements, displacement must be reconstructed by numerical integration of acceleration records, a procedure that may introduce low-frequency drift, cumulative errors, and noise amplification, especially when weak ambient vibrations are analysed. This limitation becomes particularly relevant in output-only identification of global structural modes, where the most informative response often lies in the low-frequency band [27], [28]. In addition, piezoelectric accelerometers are intrinsically unsuitable for static or very low-frequency measurements because of charge decay effects [29], [30], while piezoresistive accelerometers may suffer from temperature-dependent sensitivity and higher noise levels [24]. Capacitive MEMS accelerometers can operate down to DC, and are attractive because of their compactness, but they still remain acceleration-based devices and may be more sensitive to environmental variations and metrological constraints when displacement is the target variable [31], [32]. By contrast, broadband seismometric sensors are specifically designed to provide high sensitivity in the low-frequency range, with flat response characteristics over a broad spectrum and improved capability to resolve weak motion signatures. For these reasons, a displacement-sensitive broadband mechanical seismometer was considered more appropriate, because it directly provides a displacement-related output, avoids double integration, and ensures higher robustness and reliability in the measurement chain for ambient-vibration-based modal identification.

A distinctive feature of this class of sensors, compared with other commonly used technologies (e.g. laser scanners), lies in the physical principle of measurement. The folded-pendulum architecture effectively realises an inertial mass above its natural resonance frequency. As a result, the measured quantities, referred to this inertial mass, correspond to absolute displacement measurements. These are not limited by the mechanical structure of the sensor, whose fundamental limit is given by thermal noise and damping effects due to air, but rather by the performance of the readout system. In the present case, the readout is based on an electromagnetic LVDT system; however, alternative implementations within the same class of sensors may employ interferometric readout, achieving sensitivity improvements of several orders of magnitude.

At frequencies below the resonance frequency, the behaviour differs. Since no feedback control system is employed—unlike most commercial displacement or acceleration sensors—the signal depends on the capability of the readout system to limit electronic noise, typically characterised by a $1/f$ behaviour. The mechanical system remains fundamentally limited by thermal noise, while the sensitivity decreases with a slope of approximately 40 dB/decade, as expected for second-order oscillatory systems. Consequently, the overall performance in the low-frequency range is determined primarily by the readout electronics, rather than by the mechanical architecture.

Although more advanced interferometric solutions are available, the choice of this class of sensors was considered adequate for this initial measurement campaign. However, it is important to emphasise that sensor technology does not represent a limiting factor for the DFEM procedure. Should higher sensitivity or broader bandwidth be required—particularly for more complex structural configurations—the system can be readily upgraded by employing alternative sensors within the same class, featuring lower resonance frequencies and improved readout technologies, such as quadrant photodiodes or Michelson-type interferometric systems.

Unlike many conventional accelerometric systems, these seismometers provide both the sensitivity and bandwidth necessary to capture the true dynamic behaviour of the bridge, including very low-frequency modal peaks, linear and angular displacements, and day–night cyclic deformations. Their metrological performance proved essential for identifying resonance frequencies and for distinguishing structural behaviour from environmental or transient perturbations.

Figure 4 reports, for illustrative purposes, the displacement-noise curves of a GM24 monolithic folded pendulum tuned to $f_0 = 250$mHz.

This oscillator is not the SE-10HL sensor used in the Savuto River bridge measurements but provides a representative example of the operating principles and performance limits of the folded-pendulum architecture. Above the resonance frequency, the central mass behaves approximately as an inertial reference; the resonance therefore defines the transition to the inertial operating range, rather than an absolute measurement limit. The practical sensitivity is mainly governed by the intrinsic noise of the adopted readout, whereas the ultimate mechanical limit is set by the thermal noise of the oscillator, as described by the fluctuation–dissipation theorem. The curves compare different readout technologies with the Peterson New Low Noise Model [33] and the McNamara and Buland noise model [34].

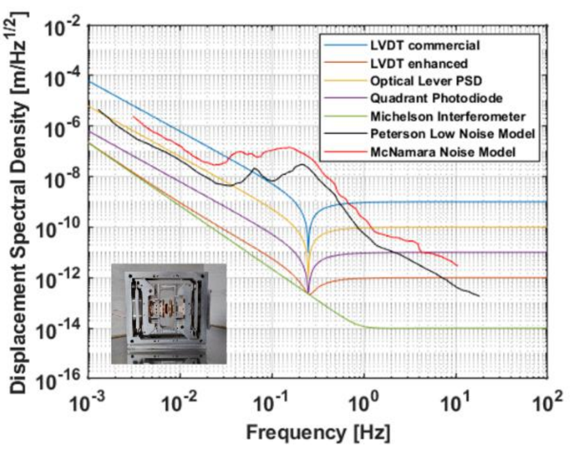

Figure 4. Sensitivity curves for the monolithic Folded Pendulum, Model GM24, tuned at f_o=250 mHz for different typologies of readouts, compared with the Peterson Low Noise Model [33] and with the McNamara Noise Model [34].

3.2. System installation

The installation strategy was explicitly designed to be non-invasive. The sensors were placed directly on the bridge roadway and mechanically stabilised using stone support elements positioned between the sensor bases and the monument surface (see Figure 5 and Figure 6). This approach, previously validated in both permanent and temporary monitoring campaigns, ensured effective coupling between the sensors and the structure, while fully respecting conservation requirements. No invasive anchoring systems were employed, and the installation remained entirely reversible.

The spatial distribution of the sensors was progressively refined throughout the DFEM optimisation process. Their positioning was designed to maximise sensitivity to the principal dynamic modes of the structure, and to enable the simultaneous measurement of translational and rotational responses in critical regions of the deck and piers. This adaptive deployment was particularly important, as one of the objectives of the procedure was to determine the number of structural degrees of freedom required for an accurate dynamic representation of the bridge. In this sense, the monitoring system did not merely record behaviour but actively contributed to defining the structural complexity of the system under investigation.

Figure 5. Couple of mechanical seismometers positioned on the roadway of the Roman bridge.

Figure 6. Details of installed seismometers. The stone elements on which the sensors were positioned, acting as support base, guarantee a perfect sensor stability and the quality of the measurements.

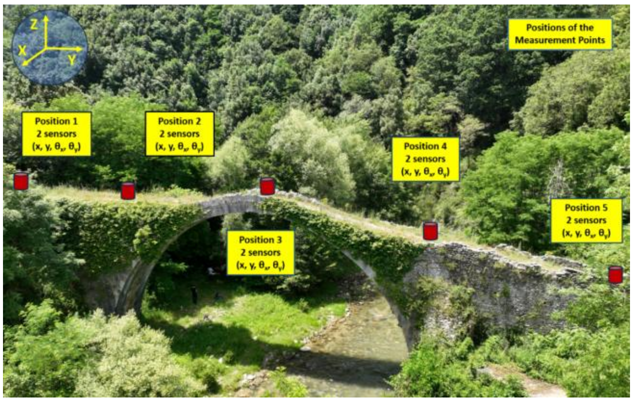

Figure 7. Positions of the two-dimensional measurement points on the roadway of the Roman bridge after the mutual optimization procedural step.

Considering the orientation of the bridge (39°07'58.45" N, 16°16'28.43" E), with the longitudinal section of the bridge oriented approximately 30° clockwise from the north (NNE), after the mutual optimization procedure, the sensors were moved to their final positions, schematized in Figure 7.

Each measurement point included two non-feedback horizontal seismometers, oriented at 30° N-NE along the longitudinal direction and at 120° E-SE along the transverse direction. Each sensor provided a single composite output containing both translational and tilt-induced contributions, from which the corresponding translational and rotational response components were separated during post-processing. Thus, four response components—two translational and two rotational—were reconstructed at each measurement point. Additional points on the bridge would not add significant data due to signal correlation. The monitoring system, including data archiving and power supply, was installed on the south embankment by the Sant'Angelo church, with sensors on the bridge roadway.

3.3. Experimental data analysis

For the case under study, based on the existing system components and architecture, the data were elaborated with the aid of MATLAB software, distributed by MathWorks. In particular, the raw data, stored in native *.tdms format, were initially converted into temporal sequences with a script implemented in MATLAB environment [35]. Then, the instrumental noise was removed through a deconvolution process available from the literature, being specifically implemented for broadband seismometers [33]. Then, the displacement records were analysed both in the spatial domain and in the frequency domain. The input data consisted of a matrix $\mathbf{X}(t)$, where each column represents the displacement time history measured by one broadband mechanical seismometer. For each sensor, the measured displacement signal was treated as the superposition of two physically different contributions: a translational component, associated with the actual horizontal motion of the sensor base, and an apparent low-frequency component associated with angular motion, or tilt, of the instrument.

This separation is physically justified by the operating principle of horizontal mechanical broadband seismometers. These instruments behave as inertial pendulum systems and are primarily designed to measure translational ground motion along their sensitive axis. However, horizontal pendulum-type sensors are also sensitive to tilt, because a rotation of the sensor base produces a projection of the gravitational acceleration along the nominal horizontal sensing direction. For small tilt angles θ, this apparent acceleration is approximately $g\,\theta$, where g is the gravitational acceleration. Therefore, the output of a horizontal broadband seismometer cannot be interpreted as a purely translational signal at very low frequencies, where tilt–gravity coupling may become dominant [34], [36], [37]. This effect is particularly relevant for long-period signals and for displacement records obtained from broadband inertial sensors. Because the adopted folded-pendulum sensors operate without feedback, the output of each horizontal unit is the superposition of the translational displacement of the sensor base and the response induced by angular motion. These contributions can be separated using two complementary approaches. In the conventional frequency-domain approach adopted here, the tilt-dominated response occurs at frequencies substantially lower than the translation-dominated response. Thus, the two components can be identified and separated when their spectral bands do not significantly overlap. An independent analytical check can also be performed by exploiting the tilt-induced shift of the folded-pendulum resonance frequency. For this sensor architecture, the resonance shift provides an estimate of the rotational contribution, which can be removed from the total output to recover the translational component. This second procedure and its physical basis are described in a previous research work [38].

In this study, which refers to the use of broadband seismometers, we adopted a method to compute the tilt from the displacement signal derived from the literature [39], [40]. In the frequency domain, the relation between displacement and acceleration allows the tilt-related part of the signal to be expressed in angular units. If $U_{\mathrm{tilt}}(f)$ is the displacement component attributed to tilt–gravity coupling, the corresponding apparent acceleration is:

$$A_{\mathrm{tilt}}(f) = -(2\,\pi\,f)^2 U_{\mathrm{tilt}}(f), \tag{4}$$

and, assuming that this apparent acceleration is mainly due to the projection of gravity, $A_{\mathrm{tilt}}(f) \simeq g\,\Theta(f)$, so that the angular displacement can be estimated as:

$$\Theta(f) \simeq -\frac{(2\,\pi\,f)^2}{g} U_{\mathrm{tilt}}(f), \tag{5}$$

where $\Theta(f)$ is the angular displacement spectrum. This formulation avoids the direct and dimensionally incorrect conversion of displacement into angle by division by g. Instead, the low-frequency displacement component is first interpreted as an equivalent tilt-induced displacement and is then converted into angular displacement through the dynamic relationship between displacement, acceleration, and tilt.

Operationally, for each sensor, the displacement signal was transformed into the frequency domain. A low-frequency band, where the response is expected to be affected mainly by tilt–gravity coupling and long-period instrumental effects, was separated from the higher-frequency band, where the signal is assumed to be dominated by translational motion. The separation frequency was identified from the spectral behaviour of the signal, using the slope of the power spectral density as an indicator of the transition between tilt-dominated and translation-dominated regimes. The low-frequency component was then transformed into an equivalent angular displacement, while the complementary component was retained as the translational displacement.

Next, the dynamic identification was performed using an output-only operational modal analysis approach. In this framework, modal parameters are estimated from the measured structural response alone, without measuring or applying a known input force. This is particularly appropriate for ancient masonry bridges and other heritage structures, where artificial excitation may be impractical, invasive, or not representative of real operating conditions. Instead, the method exploits naturally available ambient and operational actions, such as micro-tremors, wind, traffic, and environmental vibrations, which act as broadband stochastic excitation sources. This principle is well established in operational modal analysis of civil engineering and heritage structures.

Although masonry structures may exhibit nonlinear behaviour due to cracking, contact phenomena, and material or interface heterogeneity, the very low amplitude of the natural microtremor and ambient excitation allows the measured response to be treated as a small-signal linearisation around the current equilibrium state. This assumption does not exclude nonlinear mechanisms at higher excitation levels but makes the linear state-space formulation adopted in SSI-COV mechanically reasonable under the investigated operational conditions. The high sensitivity and low-frequency performance of the broadband seismometers are essential in this respect, as they allow modal information to be extracted without applying stronger artificial excitation that could activate nonlinear structural mechanisms.

In the present case, the adopted broadband seismometers provided the sensitivity required to resolve very low-amplitude displacement responses over the frequency range of interest. For massive masonry structures, whose ambient vibration levels may be small, such sensors improve the signal-to-noise ratio and make it possible to identify modal parameters under real boundary and operational conditions. Similar approaches have been used in long-term ambient vibration monitoring of historical masonry towers, where high-sensitivity instrumentation allowed the dynamic behaviour of structures with very low vibration levels to be followed reliably [41].

In detail, the dynamic response of the masonry bridge was analysed under operational conditions, using the displacement time histories recorded by a set of broadband seismometers. Then, the selected identification method was Covariance-driven Stochastic Subspace Identification (SSI-COV) [42]. The measured output matrix was defined as:

$$\mathbf{Y} = \begin{bmatrix} y_1(1) & y_2(1) & \cdots & y_M(1) \\ y_1(2) & y_2(2) & \cdots & y_M(2) \\ \vdots & \vdots & \ddots & \vdots \\ y_1(N) & y_2(N) & \cdots & y_M(N) \end{bmatrix} \in \mathbb{R}^{N\times M}\,, \tag{6}$$

where N is the number of time samples and $M = 10$ is the number of sensors. Each column of $\mathbf{Y}$ contains the displacement response, expressed in metres, measured at one sensor location. The sampling frequency, f_s, corresponds to a sampling interval:

$$\Delta t = \frac{1}{f_s}\,. \tag{7}$$

Before identification, the signals were detrended in order to remove constant and linear components that may bias the covariance estimates, especially at very low frequencies. This operation is particularly relevant for field measurements on ancient masonry structures, where long-period components may include environmental drift, soil-foundation interaction effects, or non-structural trends, rather than true vibration modes.

The output-only system was represented in discrete-time stochastic state-space form as:

$$\mathbf{x}_{k+1} = \mathbf{A}\mathbf{x}_k + \mathbf{w}_k, \tag{8}$$

$$\mathbf{y}_k = \mathbf{C}\mathbf{x}_k + \mathbf{v}_k\,, \tag{9}$$

where $\mathbf{x}_k$ is the state vector, $\mathbf{y}_k \in \mathbb{R}^M$ is the measured output vector, $\mathbf{A}$ is the discrete-time state matrix, $\mathbf{C}$ is the output matrix, and $\mathbf{w}_k$, $\mathbf{v}_k$ are process and measurement noise terms. Since the input excitation is not measured, the identification is based only on the output covariance sequence, as customary in operational modal analysis and stochastic subspace identification.

For each positive time lag i, the output covariance matrix was estimated as

$$\mathbf{R}_i = \mathbb{E}[\mathbf{y}_{k+i}\mathbf{y}_k^T] \approx \frac{1}{N-i}\sum_{k=1}^{N-i} \mathbf{y}_{k+i}\,\mathbf{y}_k^T\,. \tag{10}$$

The covariance matrices were then assembled into a block Toeplitz matrix:

$$\mathbf{T}_s = \begin{bmatrix} \mathbf{R}_0 & \mathbf{R}_1 & \cdots & \mathbf{R}_{s-1} \\ \mathbf{R}_1 & \mathbf{R}_0 & \cdots & \mathbf{R}_{s-2} \\ \vdots & \vdots & \ddots & \vdots \\ \mathbf{R}_{s-1} & \mathbf{R}_{s-2} & \cdots & \mathbf{R}_0 \end{bmatrix}, \tag{11}$$

where s is the number of block rows. In the adopted implementation, s was chosen proportional to the maximum investigated system order, namely:

$$s = 2\,n_{\max}\,. \tag{12}$$

This choice provides a sufficiently large covariance horizon for the identification of low-frequency modes, while avoiding an excessive increase in the dimension of the Toeplitz matrix. For the present analysis, the maximum system order was set to $n_{\max} = 80$, and the tested model orders were $n = 10, 12, 14, \ldots, 80$. The use of a range of model orders is necessary, because, in stochastic subspace identification, physical modes are expected to persist when the model order is increased, whereas numerical or noise-related poles tend to appear only at isolated orders. This principle is the basis of the stabilization diagram commonly used in operational modal analysis.

For each model order n, the block Toeplitz matrix was decomposed by singular value decomposition:

$$\mathbf{T}_s = \mathbf{U}\,\mathbf{\Sigma}\,\mathbf{U}^T\,. \tag{13}$$

The order-n approximation was obtained by retaining the first n singular values and singular vectors,

$$\mathbf{U}_n = [\mathbf{u}_1 \quad \mathbf{u}_2 \quad \cdots \quad \mathbf{u}_n], \mathbf{\Sigma}_n = \mathrm{diag}(\sigma_1, \sigma_2, \ldots, \sigma_n). \tag{14}$$

The extended observability matrix was then estimated as

$$\mathbf{\Gamma}_{s,n} = \mathbf{U}_n \mathbf{\Sigma}_n^{1/2}. \tag{15}$$

The discrete-time state matrix was obtained from the shift-invariance property of the observability matrix. By removing the last block row and the first block row of $\mathbf{\Gamma}_{s,n}$, respectively, two shifted matrices were defined:

$$\mathbf{\Gamma}_1 = \mathbf{\Gamma}_{s,n}(1{:}\,M(s-1), :), \tag{16}$$

$$\mathbf{\Gamma}_2 = \mathbf{\Gamma}_{s,n}(M+1{:}\,Ms, :). \tag{17}$$

The state matrix was estimated in the least-squares sense as

$$\mathbf{A}_n = \mathbf{\Gamma}_1^{\dagger}\mathbf{\Gamma}_2 \, . \tag{18}$$

The output matrix was obtained from the first block row of the observability matrix:

$$\mathbf{C}_n = \mathbf{\Gamma}_{s,n}(1{:}\,M,:). \tag{19}$$

The eigenvalue problem is as follows:

$$\mathbf{A}_n \, \boldsymbol{\psi}_r = \mu_r \, \boldsymbol{\psi}_r \, , \tag{20}$$

provided the discrete-time eigenvalues μ_r and eigenvectors $\boldsymbol{\psi}_r$. The corresponding continuous-time eigenvalues were computed as:

$$\lambda_r = \frac{\ln(\mu_r)}{\Delta t} = f_s \ln(\mu_r). \tag{21}$$

In this expression, λ_r is the continuous-time complex pole associated with the r-th vibration mode. It is obtained from the discrete-time eigenvalue μ_r of the identified state matrix through the logarithmic mapping $\lambda_r = \ln(\mu_r)/\Delta t$. Its real part describes the modal decay rate, whereas its imaginary part gives the damped circular frequency of the mode. Accordingly, the modal frequency and damping ratio are computed as $f_r = | \operatorname{Im}(\lambda_r) | / (2\,\pi)$ and $\xi_r = -\operatorname{Re}(\lambda_r) / | \lambda_r |$, respectively.

The natural frequency and damping ratio of the r-th pole were then obtained as

$$f_r = \frac{| \operatorname{Im}(\lambda_r) |}{2\,\pi}, \tag{22}$$

$$\xi_r = -\frac{\operatorname{Re}(\lambda_r)}{| \lambda_r |}. \tag{23}$$

The associated mode shape was estimated as

$$\boldsymbol{\phi}_r = \mathbf{C}_n \boldsymbol{\psi}_r \, . \tag{24}$$

The modal vector in the measurement coordinates was obtained as $\boldsymbol{\phi}_r = \mathbf{C}_n \boldsymbol{\psi}_r$, where $\boldsymbol{\psi}_r$ is the eigenvector of the identified state matrix associated with the r-th pole, and $\mathbf{C}_n$ is the output matrix estimated at model order n. Therefore, $\boldsymbol{\phi}_r$ represents the operational mode shape projected onto the sensor coordinates, with one component for each measured output channel.

Each mode shape was normalised as

$$\hat{\boldsymbol{\phi}}_r = \frac{\boldsymbol{\phi}_r}{\| \boldsymbol{\phi}_r \|_2}. \tag{25}$$

Only poles with positive frequency and physically admissible damping were retained for subsequent interpretation. In particular, negative damping values were not accepted as physical modal parameters, even when the corresponding pole satisfied numerical stabilization criteria. This distinction is important because stabilization indicates persistence of a pole across model orders, but it does not by itself guarantee physical admissibility.

After this preliminary extraction, the set of poles identified at each model order was not directly interpreted as a set of physical modes. Instead, a stabilization procedure was applied in order to distinguish structural poles from numerical or noise-related poles [43]. This step is necessary because the SSI-COV algorithm produces a number of poles that increases with the assumed model order, and only the poles associated with physical vibration modes are expected to remain stable when the order is progressively increased.

In the adopted procedure, each pole identified at model order n_k was compared with the poles identified at the previous model order n_{k-1}. A pole was classified as stable only when a triple stabilization criterion was simultaneously satisfied, involving natural frequency, damping ratio and mode-shape consistency. This criterion corresponds to the stabilization logic implemented in the MATLAB procedure, where stable modes are selected by checking frequency variation, damping variation and Modal Assurance Criterion (MAC) between mode shapes across consecutive model orders.

The relative frequency difference between two candidate poles was defined as:

$$\delta_{\mathrm{f}} = \frac{\left| f_r^{(k)} - f_q^{(k-1)} \right|}{f_q^{(k-1)}}. \tag{26}$$

The frequency stability condition was imposed as $\delta_{\mathrm{f}} \le \varepsilon_{\mathrm{f}}$. In the updated analysis, the threshold was set to $\varepsilon_{\mathrm{f}} = 0.0075$. This value is slightly more restrictive than the commonly adopted 1 % tolerance. The choice was made because frequency is generally the most robust modal parameter in output-only modal identification, whereas damping is more affected by the uncontrolled nature of ambient excitation and by measurement noise. Therefore, a slightly stricter frequency threshold helps reduce the number of closely spaced numerical poles without imposing unrealistic laboratory-type constraints on field data.

The damping stability condition was expressed through a mixed relative-absolute criterion:

$$| \xi_r^{(k)} - \xi_q^{(k-1)} | \le \max\left[\varepsilon_{\xi,\min}, \varepsilon_{\xi,\mathrm{rel}} \max\left(| \xi_q^{(k-1)} |, \varepsilon_{\xi,\min} \right)\right]. \tag{27}$$

The adopted values were $\varepsilon_{\xi,\mathrm{rel}} = 0.20$ and $\varepsilon_{\xi,\min} = 0.002$. This means that a 20 % relative variation in damping was accepted, with a minimum absolute tolerance of 0.2 % in damping ratio. This formulation was preferred to a purely absolute damping threshold because damping estimates are less stable than natural frequencies in operational modal analysis. In particular, for in-situ measurements on massive masonry structures, the estimated damping may be influenced by environmental excitation, soil-foundation interaction, local frictional mechanisms, non-structural components, and signal processing effects.

Mode-shape consistency was evaluated through the Modal Assurance Criterion:

$$\mathrm{MAC}\left(\boldsymbol{\phi}_r^{(k)}, \boldsymbol{\phi}_q^{(k-1)}\right) = \frac{| \left(\boldsymbol{\phi}_r^{(k)}\right)^H \boldsymbol{\phi}_q^{(k-1)} |^2}{\left[\left(\boldsymbol{\phi}_r^{(k)}\right)^H \boldsymbol{\phi}_r^{(k)}\right]\left[\left(\boldsymbol{\phi}_q^{(k-1)}\right)^H \boldsymbol{\phi}_q^{(k-1)}\right]}. \tag{28}$$

The mode-shape stability condition was

$$\mathrm{MAC}\left(\boldsymbol{\phi}_r^{(k)}, \boldsymbol{\phi}_q^{(k-1)}\right) \ge \varepsilon_{\mathrm{MAC}} \, . \tag{29}$$

The adopted value was $\varepsilon_{\mathrm{MAC}} = 0.95$. This threshold was selected to ensure that a pole stable in frequency also exhibits a consistent spatial deformation pattern across consecutive model orders. This is important because frequency stability alone may retain numerical poles or local effects that do not correspond to a well-defined global mode of the bridge.

Therefore, a pole was considered stable only if these three conditions were simultaneously fulfilled. In particular, only poles satisfying this triple criterion were marked as stable in the stabilization diagram. In addition, negative damping values were excluded from the final interpretation, since they are not physically admissible for the free vibration modes of a passive structural system.

To avoid retaining isolated poles that satisfy the criterion only locally, a persistence requirement was also introduced. A modal candidate was retained only if stable poles belonging to the same modal family appeared in at least four model orders.

This additional condition reflects the expected behaviour of physical modes in a stabilization diagram: a real mode should form a stable vertical alignment over several model orders, whereas spurious poles generally appear only at isolated orders.

Finally, stable poles were grouped into representative modes. Two stable poles were assigned to the same modal cluster only if they were close in frequency and had similar mode shapes:

$$\frac{| f_i - f_j |}{\min(f_i, f_j)} \leq \varepsilon_{\mathrm{f,cl}} , \tag{30}$$

$$\mathrm{MAC}\left(\boldsymbol{\phi}_i, \boldsymbol{\phi}_j\right) \geq \varepsilon_{\mathrm{MAC,cl}} . \tag{31}$$

The adopted clustering thresholds were $\varepsilon_{\mathrm{f,cl}} = 0.02$ and $\varepsilon_{\mathrm{MAC,cl}} = 0.90$. The frequency clustering tolerance was deliberately larger than the stabilization tolerance because it was used to merge repeated estimates of the same physical mode, not to assess stability between consecutive model orders. The additional MAC requirement avoids merging physically different modes that are close in frequency. This is especially relevant for ancient masonry bridges, where arches, fill, spandrel walls, abutments, and foundations may generate coupled or closely spaced modal responses.

For each final cluster, the representative natural frequency and damping ratio were obtained as the mean values of the stable poles belonging to the cluster:

$$\bar{f}_g = \frac{1}{N_g} \sum_{i=1}^{N_g} f_i , \tag{32}$$

$$\bar{\xi}_g = \frac{1}{N_g} \sum_{i=1}^{N_g} \xi_i . \tag{33}$$

The final modal set was therefore obtained through a hierarchical process: extraction of SSI-COV poles, exclusion of physically inadmissible poles, triple stabilization across model orders, persistence checking, and final clustering into representative modes.

4. THE DIGITAL MODEL

The implementation of the DFEM procedure required also to develop the preliminary FEM model, for which data from field surveys and on-site collections were gathered. This included a high-resolution drone survey with a Mavic 3 model, equipped with multiple cameras. Images were processed using Agisoft Metashape™ to reconstruct 3D images, following methods previously described in the literature [44]. On this basis, a 3D geometric model of the bridge was created in IperSpace BIM by Soft.Lab™. Although drone photogrammetry provides a 3D reconstruction of the visible surfaces, it cannot identify the geometrical characteristics of the volume bounded by the 3D surface, for which mass distribution, materials, voids, interfaces (e.g. soil-structure), and other relevant parameters remain unknown. This is why an optimization procedure is needed to mutually tune both the monitoring system configuration and the digital model mechanical parameters. Thus, these features are introduced in the preliminary FEM only as physically admissible assumptions and must be progressively constrained through the DFEM optimisation process, using a sufficient number of measurement points with adequate spatial distribution, sensitivity, and bandwidth.

Due to the bridge's non-homogeneous materials—limestone and irregular stones—the model incorporated a scaled arch structure with specific elastic moduli: 2.6×10^5 N/cm² for limestone and 8.7×10^4 N/cm² for other stones [45]. The interfaces of the bridge components were modelled as finite sliding with a 0.3 penalty parameter for friction, while materials were considered linearly elastic. Rayleigh damping was excluded, as it can underestimate structural response [46].

The masonry was represented through an equivalent continuum approach. This modelling choice is consistent with macro-modelling strategies commonly adopted for historical masonry arch bridges, where the objective is to reproduce the global stiffness, mass distribution and modal response of the structure, rather than the local interaction between individual stone blocks and joints [47]–[49]. In large and geometrically complex heritage bridges, detailed micro-modelling would require mechanical information on units, joints, interfaces, and internal fill, which is often unavailable or highly uncertain. For this reason, several studies on masonry arch bridges have adopted homogenised or macro-continuum finite element descriptions to obtain computationally feasible models suitable for global structural assessment and dynamic interpretation.

In the calculation model, masonry walls are automatically discretized into two-dimensional triangular shell finite elements, with assigned thickness and material properties, including shear deformability through the shear modulus. This modelling choice is appropriate for a global dynamic interpretation, because the objective is not to reproduce the local behaviour of each stone block, but to obtain the effective mass and stiffness distribution governing the measurable vibration response of the bridge.

In modal form, the FEM solves the undamped eigenvalue problem:

$$\mathbf{K}(\boldsymbol{\theta})\, \boldsymbol{\phi}_i = \omega_i^2\, \mathbf{M}(\boldsymbol{\theta})\, \boldsymbol{\phi}_i , \tag{34}$$

where $\mathbf{K}$ and $\mathbf{M}$ are the stiffness and mass matrices, $\boldsymbol{\theta}$ is the vector of uncertain model parameters, ω_i is the circular natural frequency of the i-th mode, and $\boldsymbol{\phi}_i$ is the corresponding numerical mode shape. Then, the computed frequency is:

$$f_i^{\mathrm{FEM}} = \frac{\omega_i}{2\,\pi} . \tag{35}$$

The uncertain parameters $\boldsymbol{\theta}$ mainly concern the effective stiffness and mass distribution of the masonry system, the boundary conditions at the abutments, and the degree of coupling between the arch, spandrel walls, fill, and foundation zones. This is essential for an ancient masonry bridge, because the visible geometry does not necessarily reveal internal discontinuities, hidden masses, past repairs, voids, or foundation arrangements.

The FEM was integrated into a Dynamic Finite Element Method (DFEM) workflow, based on mutual optimization between numerical prediction and experimental evidence. In this procedure, preliminary FEM results were used to identify the expected regions of maximum vibration amplitude and to define an initial sensor layout. Then, the output-only monitoring data were used to tune the FEM parameters, while the updated FEM response was used to refine the monitoring configuration. This mutual optimization was particularly important because the local authority allowed sensor installation only along the bridge carriageway, so the numerical model helped to make the most of the admissible measurement locations.

The comparison between numerical and experimental modal frequencies was expressed through the relative frequency deviation:

$$\Delta f_i = \frac{f_i^{\mathrm{exp}} - f_i^{\mathrm{FEM}}}{f_i^{\mathrm{FEM}}} \cdot 100\,\% \,. \tag{36}$$

5. THE ROMAN BRIDGE ON THE SAVUTO RIVER

The Roman bridge over the Savuto River (Figure 8), also known as the Bridge of Hannibal or Sant'Angelo Bridge, constitutes one of the most significant infrastructural survivals of Roman Southern Italy. Located between the municipalities of Altilia and Scigliano (Calabria region), the bridge lies along the route of the ancient Via Popilia, the Roman road connecting Capua to Reggio Calabria along the Tyrrhenian corridor. Built in the 2nd century BC, it occupies a strategic position within a landscape that historically mediated movement, communication, and territorial control.

The monument is of exceptional interest not only for its antiquity and state of preservation, but also for the constructive intelligence embedded in its structural form. The bridge consists of two concentric round arches made of dry-laid tuff and calcarenite blocks, forming a double-shell configuration in which the inner arch acts as the principal load-bearing element, while the outer arch contributes counterbalancing and stabilising functions. The main span measures approximately 21.5 metres, the structure rises around 11 metres above the riverbed, and the walking surface extends for nearly 48 metres, including the access ramps on both sides. Its width is about 3.55 metres.

This geometry reflects a highly refined engineering logic. Roman bridge construction, deeply rooted in proportional design and site-responsive practice, combined geometric order with functional necessity. In the Savuto bridge, such logic is manifested in the balance between slenderness and solidity, in the articulation of the arch system, and in the adaptation of the structure to the riverine environment. Its survival after more than two millennia strongly suggests the presence of sophisticated constructive solutions extending beyond the immediately visible portions of the monument.

The bridge is primarily built of red limestone extracted from quarries near Altilia, while the arches are formed from carefully squared blocks of calcarenite and tuff. This choice of materials was crucial to its durability, providing both mechanical resistance and long-term weathering stability. Archaeological reports and historical surveys have long suggested that the visible structure may not exhaust the bridge's full configuration. Previous investigations proposed that the foundation might extend approximately 1.5 metres below the riverbed and rest upon a platform of superimposed squared blocks around 5 metres wide and 1.5 metres high. Similarly, uncertainty remains regarding the precise configuration of the Altilia ramp, which may contain an infilled arch or internal cavity subsequently reinforced with buttresses. Earlier hypotheses even suggested the presence of an internal sheltered space within the ramp, though this remains archaeologically unconfirmed.

These uncertainties make the Savuto bridge especially suitable for a metrological investigation based on dynamic behaviour. Visible geometry alone does not provide sufficient information to reconstruct the full structural organism. If hidden masses, buried connections, or undocumented restoration effects are present, they must be inferred indirectly through their influence on the bridge's vibrational response. It is precisely at this point that the monument becomes a privileged object of DFEM analysis: not merely a preserved structure, but a repository of latent information on Roman engineering practice.

This is particularly relevant when considering the current condition of the bridge. Although it remains remarkably intact and still traversable, its present dynamic behaviour reflects not only its original construction but also later interventions, including twentieth-century restorations that may have altered local constraint conditions. The structure thus embodies a layered history in which Roman design, environmental action, and modern conservation measures coexist and interact. Understanding it requires an analytical method capable of distinguishing these overlapping contributions and relating them to both the visible and concealed structure.

For all these reasons, the Roman bridge on the Savuto River represents an ideal case study for the application of adaptive vibroacoustic modelling. It allows the assessment of structural health, the identification of anomalous dynamic behaviour, the investigation of hidden constructive features, and the formulation of historically meaningful hypotheses regarding Roman building techniques. More broadly, it demonstrates how advanced metrology can provide access to the intangible technical knowledge embedded in ancient infrastructures.

Figure 8. Image reconstruction of the Roman bridge on the Savuto River, along the Roman road known as via Popilia, taken from the drone.

6. RESULTS AND DISCUSSION

6.1. Results

The application of the DFEM procedure to the Roman bridge on the Savuto River produced a set of experimental results describing the bridge response under natural environmental excitation.

The monitoring system, installed non-invasively along the roadway, measured both linear and angular displacements, providing the physical component of a hybrid physical-digital platform in which the measured response was compared with the numerical output of the FEM. The results of the SSI-COV analysis, combined with the spectral analysis of the recorded signals, shown in Figure 9, allowed the identification of a set of

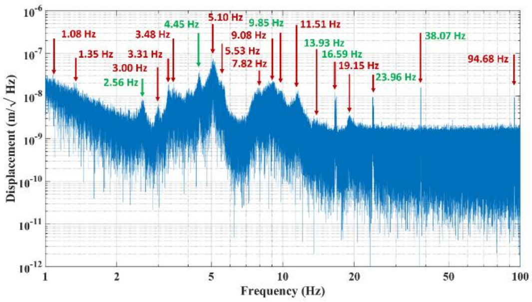

Figure 9. Structural modal frequencies (red arrows) identified from the comparison of FEM theoretical frequencies and the experimental measures on the bridge after the mutual optimization along the DFEM procedure. The comparison allows to disentangle the expected structural dynamics from the dynamics depending on the environmental excitation, as well as from any structural variable perturbation derived from the potential presence of structural damages.

stable resonance peaks associated with the global dynamic response of the bridge.

The number of dynamically observable degrees of freedom is necessarily limited by the metrological performance of the measurement chain. Resonance components falling below the sensor and readout noise floor, or outside the effective measurement bandwidth, cannot be reliably identified, and therefore cannot constrain the FEM updating process. With less sensitive sensors, several of the stable components visible in Figure 9 would not be resolved, resulting in a smaller observable modal subspace and a less constrained numerical model. Conversely, sensors with lower intrinsic noise and adequate bandwidth can reveal additional stable modal features and, provided that sufficient spatial coverage is available, increase the information supplied to the DFEM optimisation and improve the fidelity of the optimised FEM.

After the mutual optimisation between FEM and experimental data, seven principal frequencies were selected and compared with the corresponding numerical values. The results are reported in Table 3. The comparison shows a close agreement for six of the seven identified modes, with deviations generally within about 4 %. The largest discrepancy concerns the

Table 3. Theoretical (FEM) and experimental (spectral analysis for all sensors) modal frequencies after the mutual optimization process. The relative (percentage) deviations in frequency between theoretical and experimental values is reported in the right-side column.

Computed Frequency, Hz	Experimental Frequency, Hz	Relative Frequency Deviation, %
2.54	2.56	0.79
4.57	4.45	-2.63
9.87	9.85	-0.20
13.39	13.93	4.03
17.24	16.59	-3.77
21.74	23.96	10.21
38.46	38.07	1.01

mode computed at 21.74 Hz and experimentally observed at 23.96 Hz. In addition, frequency components lower than the first computed modal frequency were detected in the experimental spectra. With this respect, the high damping (8.43 %) associated with a frequency of 1.08 Hz, being lower than the first modal frequency identified through the FEM digital model, might be related to the presence of foundations, altering the soil-structure behaviour, and triggering a lower-frequency structural vibration. Instead, other frequency peaks evidenced in Figure 9 might depend on environmental excitations occurring during the measurement period.

The time-domain analysis highlighted a dominant rotational component of the bridge response. The angular displacement around the longitudinal direction (Figure 10) was more pronounced than that around the transverse direction (Figure 11). During the night, the bridge remained comparatively stable. At sunrise, the central measurement point P3 started to rotate, followed by the movement of P2. In the second measurement set, points P3, P4, and P5 showed a synchronous rotation, behaving as a coherent portion of the structure. The measured relative angular differences reached values of the order of 0.05° around the longitudinal axis, while the rotations around the transverse axis remained smaller. The angular displacement behaviour at sunrise and sunset is graphically represented in Figure 12.

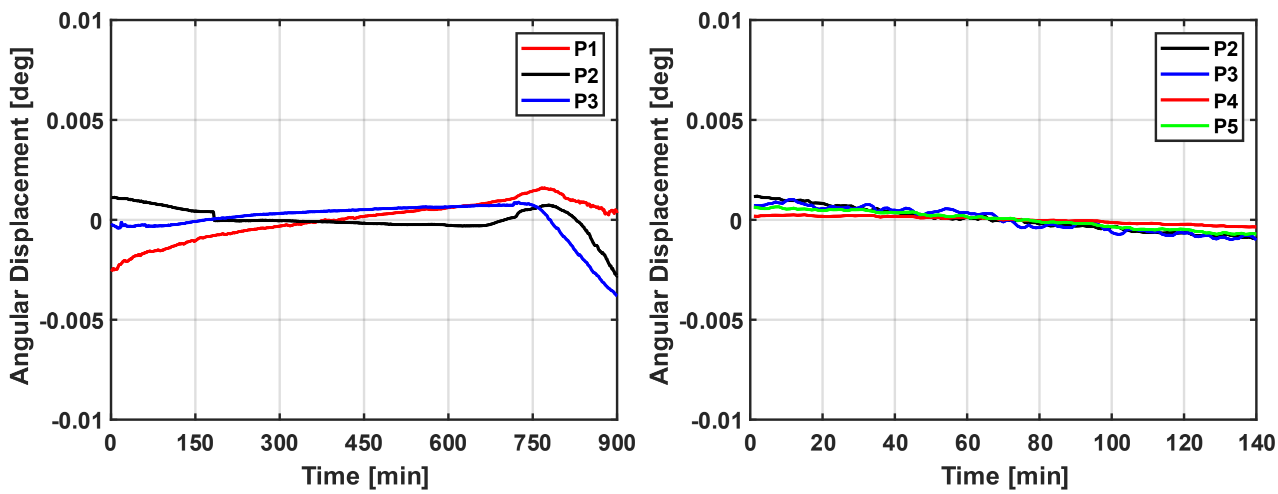

Figure 10. Angular displacement obtained from longitudinal sensors over the complete first measurement set I at P1–P3 and the complete second measurement set II at P2–P5. Sunset on June 22, together with sunrise and climax on June 23, is marked. The abscissa axes use the same units to allow comparison of the angular-displacement trend about the transverse axes throughout the monitoring interval. The rotation of the x axis is positive when clockwise (y→z).

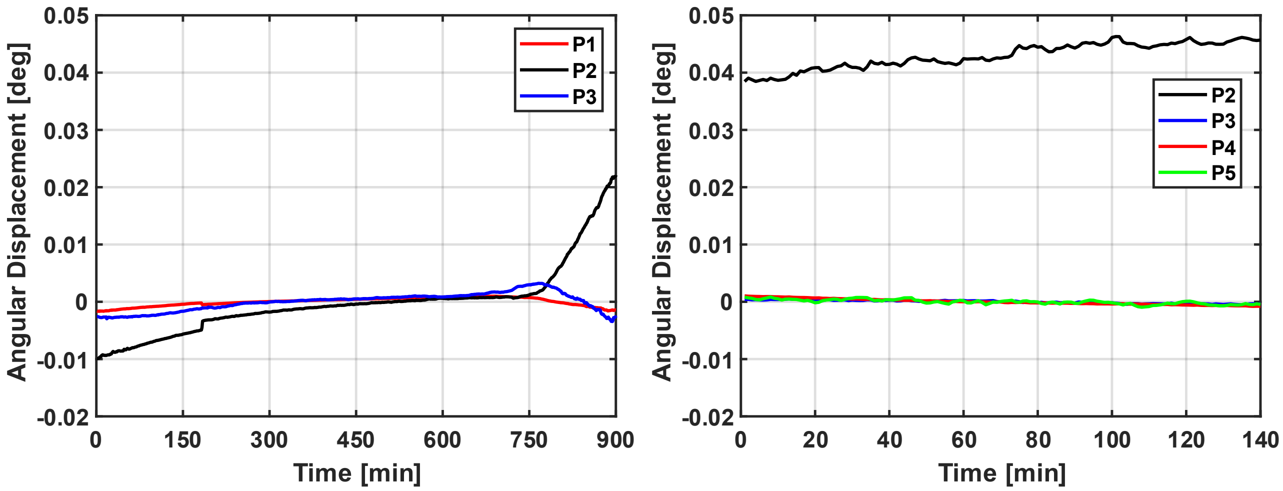

Figure 11. Angular displacement recorded by transverse sensors during the full first measurement set at P1–P3 and the full second measurement set at P2–P5. Sunset on June 22 and sunrise and climax on June 23 are indicated. Identical units are used on the abscissa axes to compare the evolution of angular displacement about the longitudinal axis over the whole monitoring period. The rotation of the y axis is positive when clockwise (x→z).

A local discontinuity was also observed at approximately $t = 150$ min in the angular records of P2 and P3. The temporal coherence of this event across sensors excludes a simple sensor readjustment effect. The same area also showed relevant features in the translational records, especially in the measurements acquired at P2.

The frequency-domain analysis of time windows extracted from the measurements (Figure 13 and Figure 14) showed a time-dependent evolution of the spectral content. In the transverse response at P2, spectral components in the 15–30 Hz range varied during the day, while a spectral concentration around 40 Hz appeared in connection with the shift or disappearance of the 38.07 Hz peak. In the longitudinal response, the spectral structure around 4 Hz became more defined after solar illumination, indicating a change in the dynamic response during thermal loading. The observed migration and redistribution of the spectral peaks are consistent with temperature-induced longitudinal and rotational movements of the bridge, which may progressively modify the opening and contact conditions of existing cracks and, consequently, the local and global stiffness of the structure.

The comparison among the spectra measured at P2, P3, P4, and P5 showed that P2 and P3 have similar dynamic behaviour, especially in the low-frequency band. Conversely, P4 showed a strong attenuation of the low-frequency components and part of the intermediate-frequency components. At P5, the low-frequency band was almost completely attenuated.

Visual inspection after the measurement campaign documented longitudinal cracks under the arch between P3 and P4, the presence of vegetation rooted in the masonry, and signs of water percolation and material washout in the southern part of the bridge.

6.2. Discussion

The results confirm that the DFEM procedure can be used as a metrological bridge between measured physical response and numerical representation. The FEM did not act as an autonomous digital replica of the monument, but as the digital component of a hybrid physical-digital platform constrained by experimental evidence. In this framework, the reliability of the

Figure 12. Angular displacement obtained from longitudinal sensors over the complete first measurement set I at P1–P3 and the complete second measurement set II at P2–P5. Sunset on June 22, together with sunrise and climax on June 23, is marked. The abscissa axes use the same units to allow comparison of the angular-displacement trend about the transverse axes throughout the monitoring interval. The rotation of the x axis is positive when clockwise (y→z).

model depends on its ability to reproduce measured modal frequencies, but also on its capacity to reveal where the visible-geometry hypothesis is incomplete.

The good agreement obtained for six of the seven principal frequencies supports the adequacy of the updated FEM for describing the global dynamic behaviour of the visible bridge structure. However, the larger discrepancy observed for the 21.74–23.96 Hz mode and the presence of frequency components below the first computed modal frequency indicate that the experimental response is not fully exhausted by the current model. These discrepancies should not be treated only as numerical errors. Within the DFEM framework, they represent metrological evidence of a possible mismatch between the visible structure and the actual dynamic system.

One mechanically admissible interpretation is the presence of additional mass, stiffness or boundary constraints associated with non-visible components beneath the riverbed.

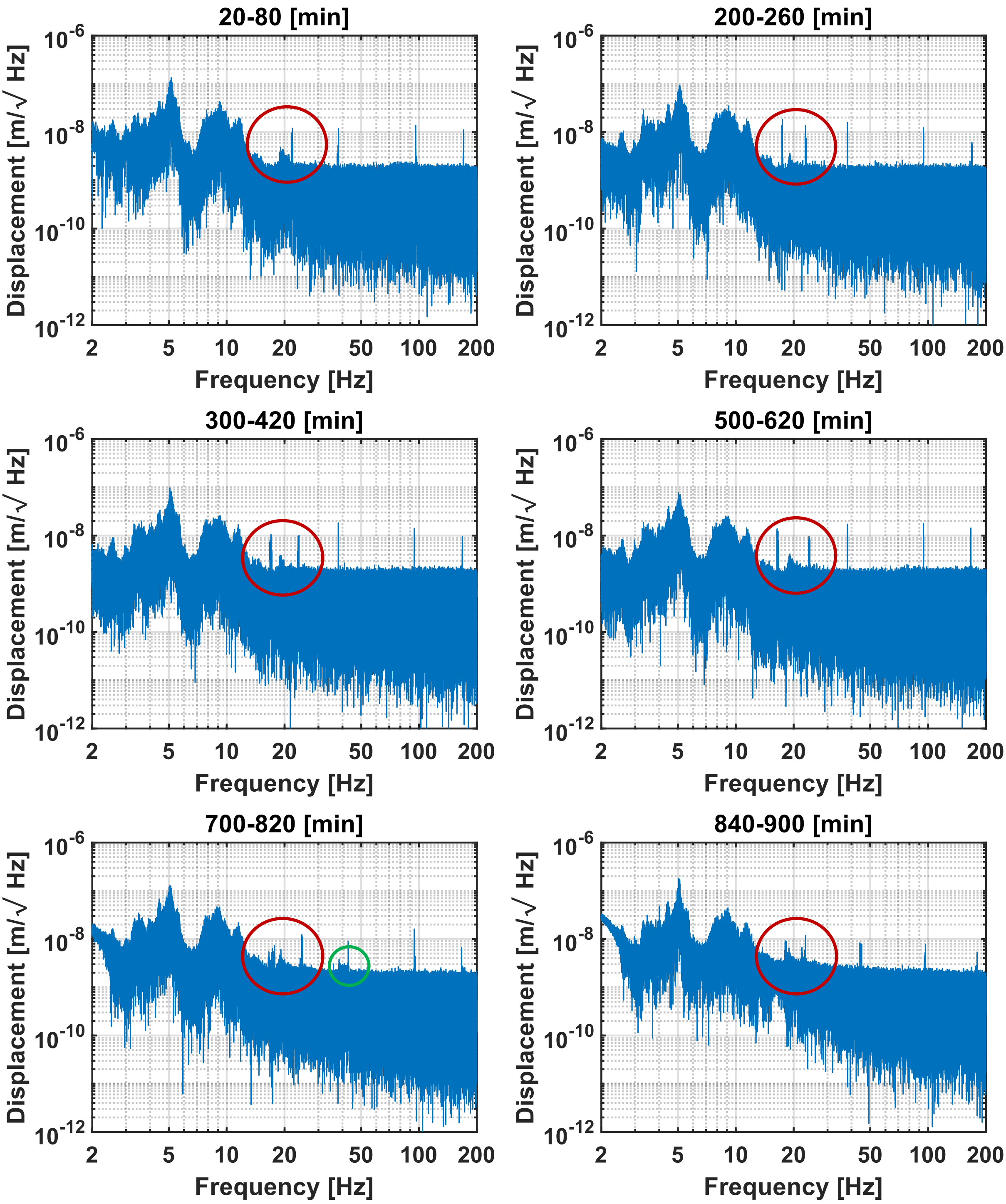

Figure 13. Evolution of the displacement-signal spectral density for the bridge transverse motion at P2 in the first data set, evaluated over one-hour time windows. The red circle highlights the time variation of spectral components in the 15–30 Hz band, interpreted as structural loosening associated with flexural cracks of variable depth and extent near the measurement point. The green circle marks the emergence of a spectral cluster around 40 Hz, concurrent with the disappearance of the 38.07 Hz peak and its shift toward higher frequencies.

This hypothesis is consistent with previous archaeological suggestions concerning a buried foundation or platform [26]. However, the present data do not constitute direct archaeological proof. They show that such a substructure is dynamically plausible, and that it should be verified through a denser sensor layout, measurements closer to the riverbed, and complementary geophysical or archaeological investigations.

The rotational response provides a second relevant outcome. The different behaviour of P2 with respect to the rest of the bridge, together with the attenuation observed at P4 and P5, suggests an asymmetric dynamic system. This asymmetry is compatible with the effects of previous restoration works, lateral embankments, and buttresses, which may have modified the original boundary conditions. In this configuration, the constrained northern side and the less constrained southern pier may respond differently to solar heating and thermal expansion.

The spectral variations observed during the day also support this interpretation. The evolution of peaks in the 15–30 Hz range and the shift of components around 38–40 Hz are compatible with local stiffness variations and possible flexural cracking

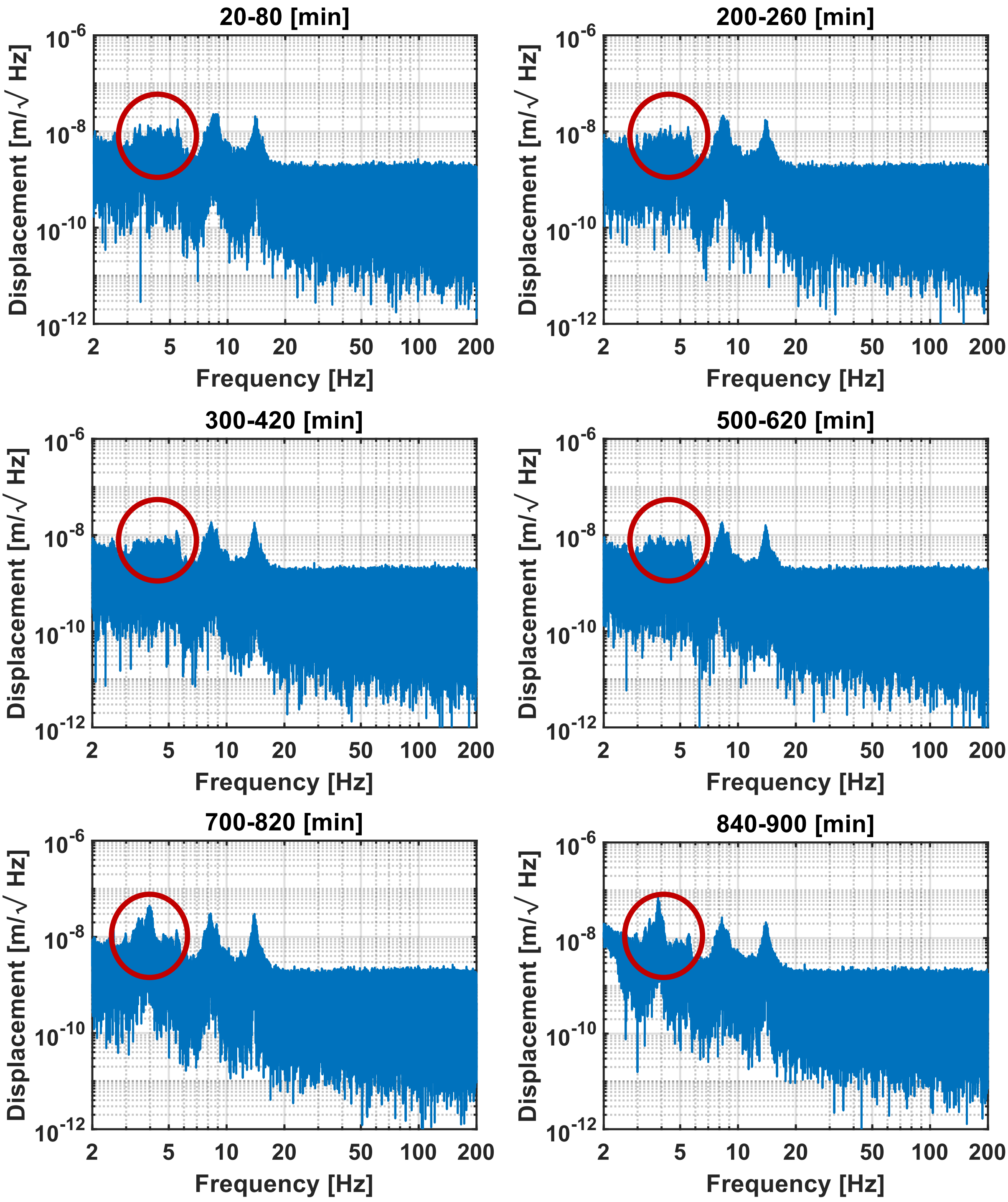

Figure 14. Evolution of the displacement-signal spectral density for the bridge longitudinal motion at P2 in the first data set, evaluated over one-hour time windows. The red circles indicate changes in the spectral pattern around 4 Hz, showing that solar-induced deformation leads to material compaction and the emergence of more clearly defined resonance modes.

phenomena [50], [51]. The observed cracks, vegetation growth, and water washout provide independent visual evidence of local vulnerability. The measurements therefore do not simply detect damage; they identify how environmental forcing activates different parts of the structure and modifies their dynamic response.

From a metrological point of view, the main result is that the high-sensitivity output-only system was able to extract relevant information without artificial excitation. This is essential for a historical masonry bridge, where active forcing would be invasive or potentially unsafe. The adopted broadband sensors allowed the physical response of the monument to be measured under real environmental conditions, overcoming the limitations previously encountered with low-cost MEMS sensors, whose sensitivity and drift issues had made artificial excitation necessary [52].

Overall, the Savuto bridge case reveals three levels of interpretation: dynamic features reproduced by the visible-geometry model, features requiring constrained model updating, and residual discrepancies requiring further investigation. This distinction is essential in heritage structures, where hidden components, altered constraints, restoration effects and limited sensor observability may coexist.

7. CONCLUSIONS

The application of the DFEM procedure to the Roman bridge over the Savuto River demonstrates the relevance of vibration metrology for cultural heritage structures whose geometry, internal configuration, materials, and boundary conditions are only partially known. The methodological contribution of DFEM lies in the integration of established principles of vibration measurement, operational modal analysis, finite element modelling, and optimisation into a single metrological procedure. In this procedure, the measurement process is not ancillary to the model: the preliminary FEM provides a first estimate for designing the sensor layout, and the measured response cyclically refines both the model parametrisation and the spatial configuration of the measurement system.

This approach is particularly important for heritage structures, where the monitoring system must be designed under conservation, access, and operational constraints that differ substantially from those of industrial or laboratory structures. Sensor installation must be non-invasive and reversible, and the number, position, and orientation of sensors are limited by the morphology and protection requirements of the monument. DFEM treats these constraints as part of the metrological problem. The final outcome is therefore not only a calibrated numerical model, but an optimised physical-digital configuration capable of identifying which dynamic features can be reliably observed and which residual discrepancies require further investigation.

The Savuto bridge case confirms the value of this approach. The comparison between measured response and numerical prediction showed that the visible geometry is not sufficient to explain all the experimentally observed dynamic features, especially in the low-frequency range. The residual discrepancies support the mechanically admissible hypothesis of additional hidden mass and/or stiffness beneath the riverbed, possibly associated with a buried foundation system connecting the main piers. This interpretation is compatible with previous archaeological hypotheses but remains a dynamically grounded hypothesis requiring further verification rather than direct archaeological proof.

The measured rotational behaviour also showed that later interventions affected the present dynamic equilibrium of the bridge. The counterphase response observed in the southern pier indicates that twentieth-century restoration works introduced asymmetric constraints and modified the original distribution of stiffness and boundary conditions. Vibration metrology therefore provides a means of distinguishing, in mechanical terms, between original structural logic, environmental adaptation, and subsequent conservation actions.

The implications of the study extend beyond structural diagnosis. DFEM shows how vibration measurements can support the investigation of complex, multimaterial, and historically transformed structures with unknown design and partially inaccessible internal organisation. In such cases, the dynamic response is one of the few available sources of integrated physical information on the real behaviour of the system. Residual discrepancies between model and measurement are not treated as numerical errors alone, but as metrological evidence that may indicate hidden structural components, insufficient observability, altered constraints, restoration effects, or undocumented construction solutions.

This makes DFEM relevant not only for the material conservation of heritage assets, but also for the interpretation of their intangible technical dimension. The Savuto bridge is material evidence of ancient téchne, understood as empirical, practice-based, and non-codified construction knowledge developed through observation, experience, material selection, and environmental adaptation. The inferred foundation system, the distribution of mass and stiffness, the adaptation to the river environment, and the long-term structural persistence of the bridge point to a refined empirical understanding of stability and load transfer. DFEM provides a contemporary metrological language for accessing this knowledge through the measured dynamic behaviour of the built form.

The study also clarifies the role of digital models in heritage science. BIM environments, digital twins, and AI-based reconstructions can support documentation and management, but they become epistemically weak if they are not constrained by high-quality measurements. DFEM transforms the digital model into a physically informed and continuously verifiable interface between the monument and its interpretation.

In conclusion, the Savuto bridge case study shows that DFEM can support a new generation of metrological applications for cultural heritage. It improves the reliability of digital models, optimises the measurement process under real conservation constraints, and enables vibration metrology to contribute to the reconstruction of both hidden structural configurations and ancient téchne embedded in historical structures.

AUTHORS' CONTRIBUTION

All the authors equally contributed to the work. Fabrizio Barone: conceptualization, formal analysis, methodology, supervision, writing – original draft; Armando Di Maio: investigation, resources, writing – review & editing; Salvatore Antonio Fornaro: investigation, resources, software, writing – review & editing; Marco Casazza: data curation, investigation, validation, writing – review & editing.

ACKNOWLEDGEMENT

The Authors thank the "Soprintendenza Archeologica Belle Arti e Paesaggio per la Provincia di Cosenza" (Italy). In particular, the Authors thank the past and the current Superintendent, dr. Paola Aurino, and the officers, architect dr. Nicola Ruggeri and archaeologist dr. Giovanna Verbicaro, for the authorization and the technical support to carry out this scientific project. The authors thank the Mayor of the Municipality of Altilia, dr. Pasquale De Rose, and the Mayor of the Municipality of Scigliano, dr. ing. Raffaele Pane, for the authorizations and the logistic supports provided to carry out this scientific project. The Authors thank also the President of the City Council of the municipality of Altilia, dr. Angela Nuccio, for her support to the research project. The authors thank dr. Gabriele Morelli for his competent and friendly support and collaboration, without which the objectives of this project would not have been achieved. Finally, the Authors wish to thank the company Advanced Scientific Sensors and Systems (Adv3S™), which kindly provided the documentation, instrumentation and acquisition software used for the measurements.

REFERENCES

[1] M. Casazza, R. Fiorillo, F. Barone, Church bells tuning temperament evaluation through spectral acoustic emission matching, Journal of Cultural Heritage 77 (2026), pp. 109–116. DOI: 10.1016/j.culher.2025.11.005

[2] F. Barone, R. Fiorillo, A. D. Maio, M. Casazza, Geometry of a Medieval Town in the Context of Political Religious Governance of the Territory, Proc. of the TC26 MetroArcheo Conference 2025 on Metrology for Cultural Heritage - MetroArcheo 2025, IMEKO, Bergamo, Italy, 15-17 October 2025, pp. 490–495. DOI: 10.21014/tc26-2025.091

[3] F. Barone, M. Casazza, Functional vibroacoustic implications of Doric temples geometrical design, Npj Herit. Sci. 13 (2025), 419. DOI: 10.1038/s40494-025-02003-3

[4] F. Barone, S.A. Fornaro, A. Di Maio, M. Casazza, The Roman Bridge on the Savuto River: understanding its dynamical structural behavior through the adaptive DFEM method, Proc. of the TC26 MetroArcheo Conference 2025 on Metrology for Cultural Heritage - MetroArcheo 2025, IMEKO, Bergamo, Italy, 15-17 October 2025, pp. 431–436. DOI: 10.21014/tc26-2025.080

[5] R. Fiorillo, A. Di Maio, S. A. Fornaro, M. Casazza, Metrological requirements for the broadband vibro-acoustic monitoring system of the San Pietro a Corte church bell tower, Salerno, Italy, AeC 13 (2025), pp. 143–157. DOI: 10.19282/acs.13.2025.11

[6] F. Barone, M. Casazza, Adaptive Modular Monitoring Systems as Interfaces with Finite Element Models in the "Phygital" Dynamic Evolution of Historical Monuments, in: F. M. Mazzolani, R. Landolfo, R., B. Faggiano (Eds.), Protection of Historical Constructions. PROHITECH 2025, Springer Nature Switzerland AG, Cham (Switzerland), 2025, pp. 505–512. DOI: 10.1007/978-3-031-87312-6_62

[7] L. Petti, F. Barone, A. Mammone, G. Giordano, Static and dynamic behaviour assessment of the Trajan Arch by means of new monitoring technologies, Int. Arch. Photogramm. Remote Sens. Spatial Inf. Sci. XLII-2/W5 (2017), pp. 567–574. DOI: 10.5194/isprs-archives-XLII-2-W5-567-2017

[8] L. Petti, F. Barone, D. Greco, G. Zuchtriegel, Innovative Structural Monitoring as Tool of Preservation and Valorisation of Monumental Architectures: The Case of Neptune Temple in Paestum (Salerno, Southern Italy), in: G.M. El-Qady, C. Margottini (Eds.), Sustainable Conservation of UNESCO and Other Heritage Sites Through Proactive Geosciences, Springer International Publishing, Cham, 2023, pp. 379–391. DOI: 10.1007/978-3-031-13810-2_20

[9] L. Petti, F. Sicignano, D. Greco, Evaluation of the dynamic and seismic response of the Neptune temple: Preliminary results, in: F. Mangone, V. Russo, G. Zuchtriegel (Eds.), L'emblema dell'eternità. Il tempio di Nettuno a Paestum tra archeologia, architettura e restauro, Edizioni ETS, 2019, pp. 177–189.

[10] M. Casazza, R. Montuori, E. Nastri, V. Piluso, F. Stochino, M. Zucca, C. Bernuzzi, M. Simoncelli, F. Barone, FEM-Based Preliminary Design of a Vibration Monitoring System in the Context of Decommissioned and Reinstalled Wind Towers, in: F. M. Mazzolani, V. Piluso, E. Nastri, A. Formisano (Eds.), Proc. of the 11th Int. Conf. on Behaviour of Steel Structures in Seismic Areas, Springer Nature Switzerland AG, Cham (Switzerland), 2024, pp. 983–995. DOI: 10.1007/978-3-031-62888-7_86

[11] M. Casazza, F. Barone, Cultural heritage structures and infrastructures vibration monitoring: vibration sensors metrological characteristics identification through finite elements modelling and simulation, Acta IMEKO 13 (2024) 2, pp. 1-9. DOI: 10.21014/actaimeko.v13i2.1800

[12] M. Casazza, F. Barone, Preliminary design of a vibration monitoring system to be installed in an archaeological heritage structure: The case of the Hera temple (Paestum, S Italy), Measurement: Sensors 38 (2025), 101760. DOI: 10.1016/j.measen.2024.101760

[13] A. Esfandiari, F. Bakhtiari-Nejad, A. Rahai, M. Sanayei, Structural model updating using frequency response function and quasi-linear sensitivity equation, Journal of Sound and Vibration 326 (2009), pp. 557–573. DOI: 10.1016/j.jsv.2009.07.001

[14] Y. B. Yang, Y. J. Chen, A new direct method for updating structural models based on measured modal data, Engineering Structures 31 (2009), pp. 32–42. DOI: 10.1016/j.engstruct.2008.07.011

[15] D. C. Kammer, Sensor placement for on-orbit modal identification and correlation of large space structures, Journal of Guidance, Control, and Dynamics 14 (1991), pp. 251–259. DOI: 10.2514/3.20635

[16] C. Papadimitriou, Optimal sensor placement methodology for parametric identification of structural systems, Journal of Sound and Vibration 278 (2004), pp. 923–947. DOI: 10.1016/j.jsv.2003.10.063

[17] X. Li, J. Antoni, M. J. Brennan, T. Yang, Z. Liu, A frequency domain blind identification method for operational modal analysis using a limited number of sensors, Journal of Vibration and Control 26 (2020), pp. 1383–1398. DOI: 10.1177/1077546319897218

[18] F. Barone, M. Casazza, Vibroacoustic characterization of a chamber music concert room in the context of the urban texture, Acta IMEKO 13 (2024), pp. 1–9. DOI: 10.21014/actaimeko.v13i2.1781

[19] F. Barone, G. Giordano, The UNISA folded pendulum: A very versatile class of low frequency high sensitive sensors, Measurement 118 (2018), pp. 339–347. DOI: 10.1016/j.measurement.2017.09.001

[20] F. Barone, G. Giordano, A new typology of DC tiltmeter based on the Watt's linkage architecture, Sensors and Actuators A: Physical 281 (2018), pp. 264–277. DOI: 10.1016/j.sna.2018.08.015

[21] F. Barone, G. Giordano, Mechanical Monolithic Inertial Sensors for Historical and Archeological Heritage Real-Time Broadband Monitoring, in: S. D'Amico, V. Venuti (Eds.), Handbook of Cultural Heritage Analysis, Springer International Publishing, Cham, 2022, pp. 1137–1166. DOI: 10.1007/978-3-030-60016-7_39

[22] C. Collette, S. Janssens, P. Fernandez-Carmona, K. Artoos, M. Guinchard, C. Hauviller, A. Preumont, Review: Inertial Sensors for Low-Frequency Seismic Vibration Measurement, Bulletin of

the Seismological Society of America 102 (2012), pp. 1289–1300. DOI: 10.1785/0120110223
[23] G. D'Emilia, A. Gaspari, E. Natale, Amplitude–phase calibration of tri-axial accelerometers in the low-frequency range by a LDV, J. Sens. Sens. Syst. 8 (2019), pp. 223–231. DOI: 10.5194/jsss-8-223-2019
[24] N. C. Yoder, D. E. Adams, Commonly used sensors for civil infrastructures and their associated algorithms, in: Sensor Technologies for Civil Infrastructures, Elsevier, 2022, pp. 51–76. DOI: 10.1016/B978-0-08-102696-0.00014-2
[25] C. Rainieri, G. Fabbrocino, G. M. Verderame, Non-destructive characterization and dynamic identification of a modern heritage building for serviceability seismic analyses, NDT & E International 60 (2013), pp. 17–31. DOI: 10.1016/j.ndteint.2013.06.003
[26] L. F. Ramos, L. Marques, P. B. Lourenço, G. De Roeck, A. Campos-Costa, J. Roque, Monitoring historical masonry structures with operational modal analysis: Two case studies, Mechanical Systems and Signal Processing 24 (2010), pp. 1291–1305. DOI: 10.1016/j.ymssp.2010.01.011
[27] B. Peeters, G. De Roeck, Stochastic System Identification for Operational Modal Analysis: A Review, Journal of Dynamic Systems, Measurement, and Control 123 (2001), pp. 659–667. DOI: 10.1115/1.1410370
[28] F. B. Zahid, Z. C. Ong, S. Y. Khoo, A review of operational modal analysis techniques for in-service modal identification, J Braz. Soc. Mech. Sci. Eng. 42 (2020), 398. DOI: 10.1007/s40430-020-02470-8
[29] T. Wu, D. You, H. Gao, P. Lian, W. Ma, X. Zhou, C. Wang, J. Luo, 8+ 2 more authors), Research Status and Development Trend of Piezoelectric Accelerometer, Crystals 13 (2023), 1363. DOI: 10.3390/cryst13091363
[30] V. Gupalov, A. Kukaev, S. Shevchenko, E. Shalymov, V. Venediktov, Physical Principles of a Piezo Accelerometer Sensitive to a Nearly Constant Signal, Sensors 18 (2018) 3258. DOI: https://doi.org/10.3390/s18103258
[31] Z. Ghemari, S. Belkhiri, S. Saad, New parameters for the capacitive accelerometer to reduce its measurement error and power consumption, Measurement: Energy 3 (2024), 100018. DOI: 10.1016/j.meaene.2024.100018
[32] V. Benevicius, V. Ostasevicius, R. Gaidys, Identification of Capacitive MEMS Accelerometer Structure Parameters for Human Body Dynamics Measurements, Sensors 13 (2013), pp. 11184–11195. DOI: 10.3390/s130911184
[33] M. M. Haney, J. Power, M. West, P. Michaels, Causal Instrument Corrections for Short-Period and Broadband Seismometers, Seismological Research Letters 83 (2012), pp. 834–845. DOI: 10.1785/0220120031
[34] P. W. Rodgers, The response of the horizontal pendulum seismometer to Rayleigh and Love waves, tilt, and free oscillations of the earth, Bulletin of the Seismological Society of America 58 (1968), pp. 1385–1406. DOI: 10.1785/BSSA0580051385
[35] B. Humphreys, ConvertTDMS (v10), (2022) Online [Accessed 3 May 2022] https://github.com/humphreysb/ConvertTDMS
[36] E. Wielandt, T. Forbriger, Near-field seismic displacement and tilt associated with the explosive activity of Stromboli, Annals of Geophysics 42 (1999) 3. DOI: 10.4401/ag-3723
[37] V. M. Graizer, Effect of tilt on strong motion data processing, Soil Dynamics and Earthquake Engineering 25 (2005), pp. 197–204. DOI: 10.1016/j.soildyn.2004.10.008
[38] F. Barone, G. Giordano, A new typology of DC tiltmeter based on the Watt's linkage architecture, Sensors and Actuators A: Physical 281 (2018), pp. 264–277. DOI: 10.1016/j.sna.2018.08.015
[39] S. Kinoshita, Tilt Measurement Using Broadband Velocity Seismograms, Bulletin of the Seismological Society of America 98 (2008), pp. 1887–1897. DOI: 10.1785/0120070230
[40] M. Wenner, K. Allstadt, W. Thelen, A. Lockhart, J. Hirschberg, B.W. McArdell, F. Walter, Seismometer Records of Ground Tilt Induced by Debris Flows, Bulletin of the Seismological Society of America 112 (2022), pp. 2376–2395. DOI: 10.1785/0120210271
[41] R. M. Azzara, M. Girardi, V. Iafolla, D. M. Lucchesi, C. Padovani, D. Pellegrini, Ambient Vibrations of Age-old Masonry Towers: Results of Long-term Dynamic Monitoring in the Historic Centre of Lucca, International Journal of Architectural Heritage 15 (2021), pp. 5–21. DOI: 10.1080/15583058.2019.1695155
[42] C. Rainieri, G. Fabbrocino, Output-only Modal Identification, in: Operational Modal Analysis of Civil Engineering Structures, Springer New York, New York, NY, 2014, pp. 103–210. DOI: 10.1007/978-1-4939-0767-0_4
[43] B. Peeters, G. De Roeck, Stochastic System Identification for Operational Modal Analysis: A Review, Journal of Dynamic Systems, Measurement, and Control 123 (2001), pp. 659–667. DOI: 10.1115/1.1410370
[44] M. Pepe, D. Costantino, N. Crocetto, A. Restuccia Garofalo, 3D modeling of roman bridge by the integration of terrestrial and UAV photogrammetric survey for structural analysis purpose, Int. Arch. Photogramm. Remote Sens. Spatial Inf. Sci. XLII-2/W17 (2019), pp. 249–255. DOI: 10.5194/isprs-archives-xlii-2-w17-249-2019
[45] S. Artese, M. De Ruggiero, A. Taliano Grasso, A. Manna, R. Zinno, The survey, the representation and the structural modeling of the S. Angelo roman bridge on the Savuto river (Scigliano, Calabria, Italy) for diagnostics and conservation aims., J. Phys.: Conf. Ser. 2204 (2022), 012095. DOI: 10.1088/1742-6596/2204/1/012095
[46] D. K. Baros, A. Papalou, Parametric Analysis of the Dynamic Response of Multi-Drum Columns, Journal of Earthquake Engineering 25 (2021), pp. 2908–2925. DOI: 10.1080/13632469.2019.1657986
[47] D. Addessi, C. Gatta, M. Nocera, D. Liberatore, Nonlinear Dynamic Analysis of a Masonry Arch Bridge Accounting for Damage Evolution, Geosciences 11 (2021), 343. DOI: 10.3390/geosciences11080343
[48] G. Meloni, M. Pourfouladi, N. Pingaro, Parametric Modelling and Nonlinear FE Analysis of Trepponti Bridge Subjected to Differential Settlements, Buildings 16 (2025), 47. DOI: 10.3390/buildings16010047
[49] P. B. Lourenço, G. Milani, A. Tralli, A. Zucchini, Analysis of masonry structures: review of and recent trends in homogenization techniques, Can. J. Civ. Eng. 34 (2007), pp. 1443–1457. DOI: 10.1139/L07-097
[50] R. Janeliukstis, A. Clark, M. Papaelias, S. Kaewunruen, Flexural cracking-induced acoustic emission peak frequency shift in railway prestressed concrete sleepers, Engineering Structures 178 (2019), pp. 493–505. DOI: 10.1016/j.engstruct.2018.10.058
[51] B. Liu, J. Yang, T. Gang, Analysis of sound and vibration interaction on a crack and its use in high-frequency parameter selection for vibro-acoustic modulation testing, Mechanical Systems and Signal Processing 143 (2020), 106835. DOI: 10.1016/j.ymssp.2020.106835
[52] S. Artese, M. Perrelli, Structural Health Monitoring of the Roman bridge S. Angelo on the Savuto river (Scigliano, Italy), by integration of a new sensor and geomatic techniques, Acta IMEKO 13 (2024) 2, pp. 1–9. DOI: 10.21014/actaimeko.v13i2.1480